Influence of geometrical parameters on the behaviour of SiC merged PiN Schottky rectifiers with junction termination extension*

Song Qing-Wen(宋庆文)†, Zhang Yu-Ming(张玉明), Zhang Yi-Men(张义门),
Zhang Qian(张 倩), Guo Hui(郭 辉), Li Zhi-Yun(李志云), and Wang Zhong-Xu(王中旭)

School of Microelectronics, Key Laboratory of Wide Band-Gap Semiconductor Materials and Devices, Xidian University, Xi'an 710071, China

(Received 17 June 2009; revised manuscript received 24 July 2009)

This paper investigates the behaviours of 4H–SiC merged PiN Schottky (MPS) rectifiers with junction termination extension (JTE) by extensive numerical simulations. The simulated results show that the present model matches the experimental data very well. The influences of the JTE design parameters such as the doping concentration and length of the JTE on the breakdown characteristics are discussed in detail. Then the temperature sensitivity of the forward behaviour is studied in terms of the different designs of 4H–SiC MPS with JTE, which provides a particularly useful guideline for the optimal design of MPS rectifiers with JTE.

Keywords: 4H–SiC, merged PiN Schottky rectifier, junction termination extension, breakdown, thermal behaviour

PACC: 7210, 7220, 7280

1. Introduction

Silicon carbide (SiC) is an attractive semiconductor material applied in high voltage, high temperature, and high frequency power devices due to its excellent electrical and physical properties.[1−3] It makes devices with excellent properties such as high power capacity, lower series resistance and lower power dissipation.[4] The merged PiN Schottky (MPS) structures have been conceived and developed to combine the inherent advantages of Schottky and PN diodes.[5] In forward bias, the PN junctions can be turned on so as to provide minority carrier injection into the N-drift regions, thus lowering the specific ON resistance, and in reverse bias, the depleted space charge regions generated by PN junctions can prevent the increase of electric field at the metal semiconductor interface, then reduce the barrier lowering and limit the leakage currents. Furthermore, a faster switching speed is obtained with respect to conventional PN diodes due to the lower stored minority charge. In the past few years, to improve the blocking characteristics of 4H–SiC MPS diodes, 4H–SiC MPS diodes with junction termination extension (JTE)[6−8] have been designed and fabricated by several groups. Although the JTE technique was used in most of their designs, few of them have systematically studied the design and optimization of JTE for 4H–SiC MPS. In addition, the forward I–V characteristics of 4H–SiC MPS diodes[8,9] have been tested with different temperatures and we find that the temperature sensitivity of the forward I–V behaviour is strongly affected by the geometrical parameters. However, this effect is rarely studied in detail and considered in their designs. This issue is essentially important to be included for the design of SiC power devices because of its power consumption and the application in high temperatures up to more than 600 K.

In this paper, numerical simulations have been performed by utilizing a two-dimensional (2D) device simulator ISE-DESSISE to study the behaviours of 4H–SiC MPS with JTE. To achieve high breakdown voltages, the design and optimization of JTE for 4H–SiC MPS have been discussed in detail by changing the JTE length, JTE doping concentration, W and S. The influences of geometrical parameters on forward characteristics are also investigated, as well as the temperature sensitivity of the forward I–V be-

*Project supported by Shaanxi 13115 Innovation Engineering Foundation (Grant No. 2008ZDKG-30) and Pre-research Project (Grant No. 51308040302).

†Corresponding author. E-mail: soqwe@126.com

© 2010 Chinese Physical Society and IOP Publishing Ltd

haviour.

2. Device model

The 2D numerical device simulator ISE-DESSIS[10] is used to simulate the characteristics of 4H–SiC MPS with JTE by solving Poisson's equation and the carrier continuity equation. The models used for 4H–SiC MPS are shown as follows:

$$\varepsilon\nabla^2\Psi = -q(p - n + N_D^+ - N_A^-) - \rho_{\rm s}, \tag{1}$$

$$\frac{\partial n}{\partial t} = \frac{1}{q}\nabla j_n - U_n = F(\psi, n, p), \tag{2}$$

$$\frac{\partial p}{\partial t} = \frac{1}{q}\nabla j_p - U_p = F(\psi, n, p), \tag{3}$$

$$j_n = -q\mu_n n\nabla\varphi_n, \tag{4}$$

$$j_p = -q\mu_p p\nabla\varphi_p, \tag{5}$$

where ψ is the intrinsic Fermi potential, N_D^+ and N_A^- are the ionized impurity concentration, $\rho_{\rm s}$ is the surface charge density, $\mu_{n(p)}$ is the electron (hole) mobility, ε is the electrical permittivity, q is the electronic charge, n and p are the electron and hole densities, $U_{n(p)}$ is the net electron–hole recombination rate, $j_{n(p)}$ is the electron (hole) current density, and $\varphi_{n(p)}$ is the electron (hole) quasi-Fermi potential.

In the breakdown model, electron and hole impact ionization coefficients can be presented as

$$\alpha_{n(p)} = a_{n(p)}\left[1 + c_{n(p)}(T - 300)\right]\exp\left(-\frac{b_{n(p)}}{E}\right), \tag{6}$$

where E is the electric field, $a_{n(p)}$, $b_{n(p)}$, and $c_{n(p)}$ are constants, $a_n = 3.25\times10^5$ cm^{-1}, $a_p = 3.25\times10^6$ cm^{-1}, $b_{n(p)} = 1.71\times10^7$ cm^{-1}, and $c_n = -3.3\times10^{-1}$ K^{-1}, $c_p = -3.3\times10^{-2}$ K^{-1}.

The incomplete impurity ionization model is considered, which means that the impurity is not fully ionized at room temperature. The ionization rate is only 75% for 4H–SiC with 10^{17} cm^{-3} N-type doping concentration at 300 K. However, the ionization rate increases with temperature and it is about 95% at 700 K for 4H–SiC with 10^{17} cm^{-3} N-type doping concentration. The concentration of ionized impurity atoms is given by

$$N_D^+ = \frac{N_D}{1 + G_D(T)\exp\left(\dfrac{E_{\rm Fn} - E_{\rm c}}{k_{\rm B}T}\right)}, \tag{7}$$

$$N_A^+ = \frac{N_A}{1 + G_A(T)\exp\left(-\dfrac{E_{\rm Fp} - E_{\rm v}}{k_{\rm B}T}\right)}, \tag{8}$$

where N_A and N_D are the acceptor and donor concentration respectively, $E_{\rm Fp}$ and $E_{\rm Fn}$ are the quasi-Fermi energies for electrons and holes respectively, $E_{\rm c}$ and $E_{\rm v}$ are the conduction band and valance band energies respectively, $G_{A/T}$ is the degeneracy factor for the impurity level, T is the lattice temperature and $k_{\rm B}$ is Boltzman's constant.

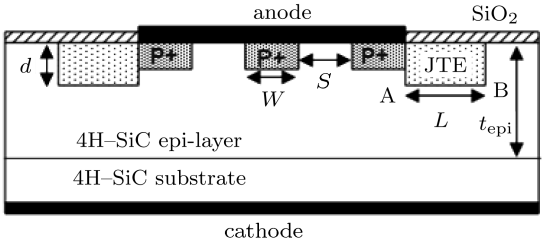


Fig. 1. Schematic cross section of a 4H–SiC MPS rectifier with JTE.

A schematic cross section of the 4H–SiC MPS diode with JTE used in the simulation is illustrated in Fig. 1. An Ni Schottky contact with a barrier height of 1.3 eV on an N-type 4H–SiC epi-layer is used. The thickness and doping concentration of the epi-layer are 18 μm and 8×10^{15} cm^{-3}, while the doping concentration of the substrate is 1×10^{19} cm^{-3}.

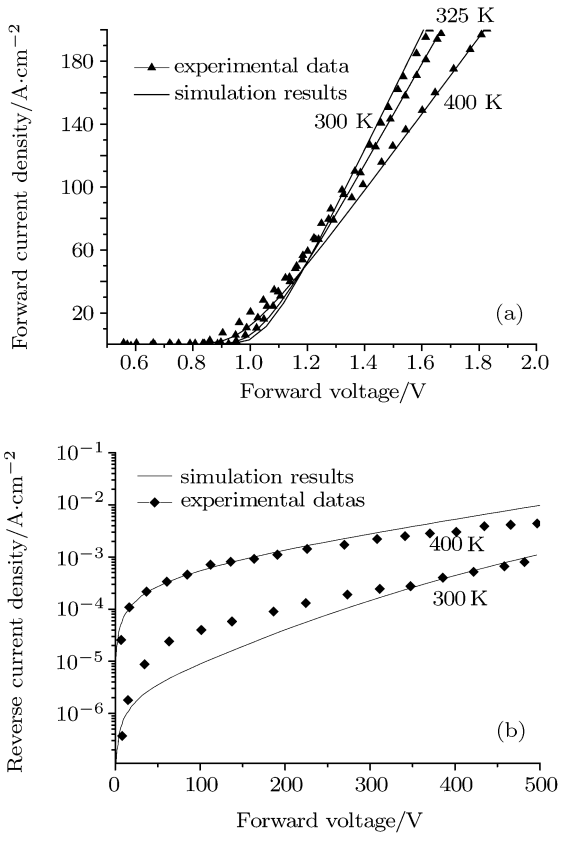


Fig. 2. Comparison of simulated forward (a) and reverse (b) I–V with experimental data from Ref. [8].

Figure 2 presents a comparison of simulated forward and reverse characteristics with experimental data[8] at different temperatures. It can be seen that the simulated results have a good agreement with the experimental data; this fact demonstrates that the present models are suitable.

3. Simulation results and discussion

As can be seen in Fig. 1, the JTE structures are designed so that they are fully depleted at the maximum blocking voltage, acting as high resistivity regions to support the high electric fields.[11] The voltage blocking capability of the 4H–SiC MPS with JTE is seriously affected by JTE design parameters such as the JTE sheet doping level ($N_{\mathrm{A-JTE}}$) and the JTE length (L), as shown in Fig. 1.

To study the influences of the JTE doping concentration ($N_{\mathrm{A-JTE}}$) on the blocking characteristics, we change $N_{\mathrm{A-JTE}}$ from 1.0×10^{17} cm^{-3} to 2.2×10^{17} cm^{-3} for four different JTE depths of 0.4, 0.6, 0.8 and 1 μm respectively. From the blocking characteristics of 4H–SiC MPS with JTE shown in Fig. 3, the breakdown voltage as a function of $N_{\mathrm{A-JTE}}$ is re-plotted in Fig. 4.

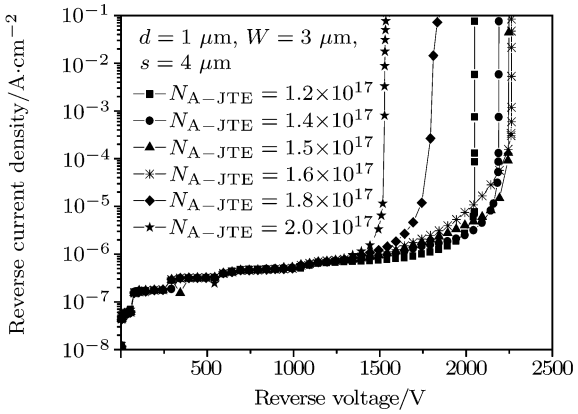


Fig. 3. Reverse characteristics for JTE terminated 4H–SiC MPS with different $N_{\mathrm{A-JTE}}$.

This indicates that a maximum breakdown voltage is reached in the concentration about 1.62×10^{17} cm^{-3}, and $N_{\mathrm{A-JTE}}$ must be precisely controlled during JTE design and process, which consistent with the design of the JTE for SiC Schottky diodes.[12] The comparison of electric field distribution along the termination for different $N_{\mathrm{A-JTE}}$ is presented in Fig. 5. At the optimum $N_{\mathrm{A-JTE}}$, the electric field distribution is relatively uniform along the termination and there are equal electric field intensities at points A and B. When $N_{\mathrm{A-JTE}}$ is beyond the optimum value, the electric field at point B increases more rapidly than that at point A.

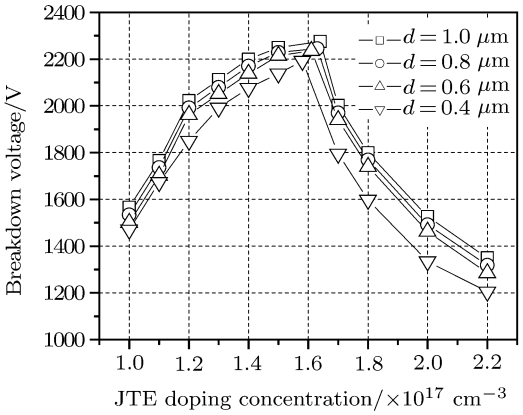


Fig. 4. The $N_{\mathrm{A-JTE}}$ dependence of the breakdown voltage for 4H–SiC MPS with different depths of JTE.

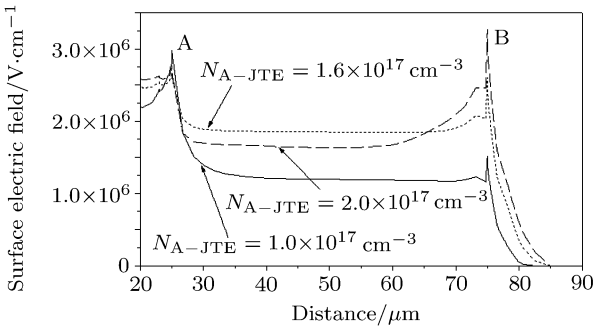


Fig. 5. Electric field distribution at breakdown along the JTE region with different JTE doping concentration.

Figure 6 presents the influence of the W and S (shown in Fig. 1) on the JTE doping concentration, which exhibits the optimum JTE doping concentration of 1.62×10^{17} cm^{-3} irrespective of the W and S. Figure 7 depicts the W and S dependence of the breakdown voltage with the optimum JTE doping concentration of 1.62×10^{17} cm^{-3}. It can be seen that the breakdown voltage of the device increases with increased W. Therefore, to achieve high breakdown voltage and small area of the device, this is an important factor to be considered in the optimal design by making a tradeoff between W and the length of the JTE.

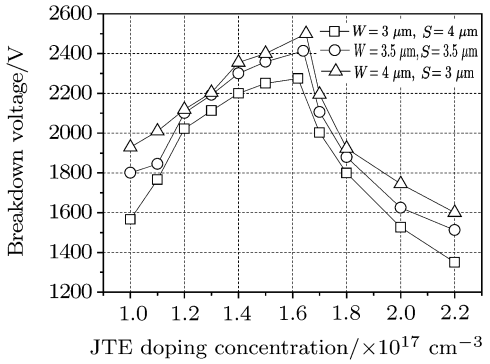


Fig. 6. The $N_{\mathrm{A-JTE}}$ dependences of the breakdown voltage for 4H–SiC MPS with different W and S.

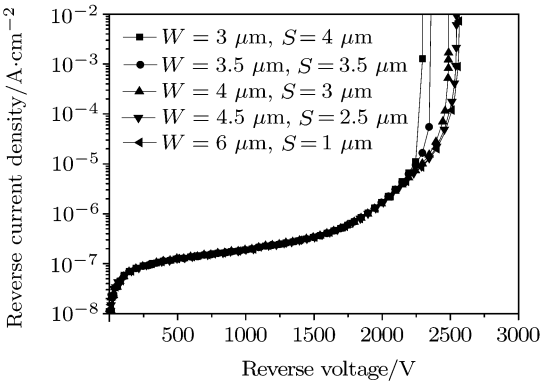


Fig. 7. Reverse characteristics for JTE terminated 4H–SiC MPS with different W and S.

Figure 8 illustrates the effect of JTE length (L) on reverse characteristics for the JTE terminated 4H–SiC MPS. The breakdown voltage vs. L is given in Fig. 9, which depicts that the breakdown voltage promptly increases with the increase of L and then

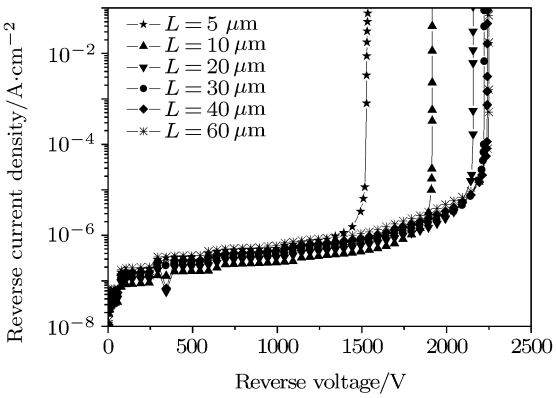


Fig. 8. Reverse characteristics for JTE terminated SiC MPS with different JTE lengths L.

begins to be saturated when L is longer than about 50 μm. At the optimum L, the electric field distribution is relatively uniform along the termination and there are equal electric field intensities at points A and B. At or beyond the optimal L, the breakdown appears nearby point A. However, the longer JTE length does not further reduce the maximum electric field near point A, so the breakdown voltage almost keeps the same value.[11] Although to some extent breakdown voltage promptly increases with the increase of L, it will lead to an increase in the area of the device at the same time. Therefore, we must make a compromise between the breakdown voltage and the area of the device during the design of the device.

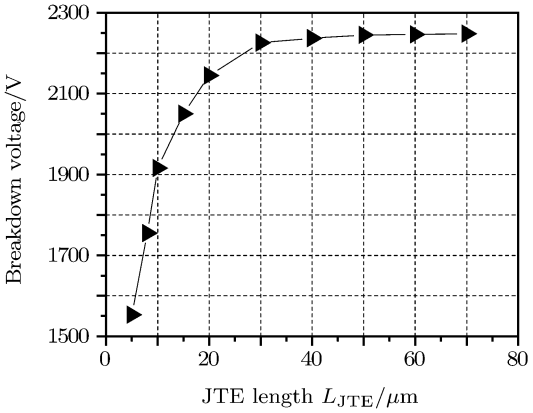


Fig. 9. The JTE length L dependence of the breakdown voltage.

Figure 10 shows the simulated forward characteristics of 4H–SiC MPS with different W and S (shown in Fig. 1) at 300 K, while keeping the sum of the W and S equal 7 μm. It can be seen that on-state voltage increases with the increase of W, while the specific ON resistance decreases with the increase of W, because the PN junction can provide more minority carriers to the N-drift region. So there is a tradeoff between the on-state voltage and specific ON resistance during the design of 4H–SiC MPS.

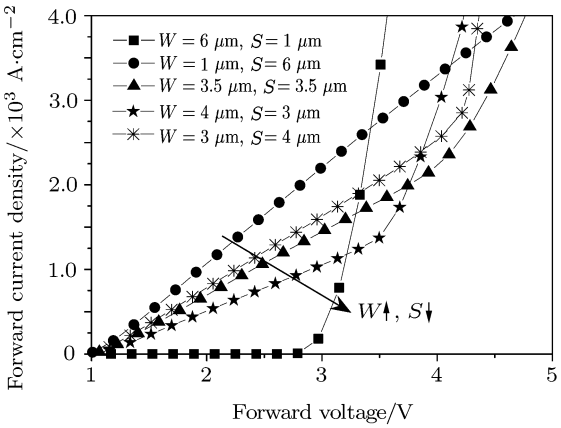


Fig. 10. Simulated forward characteristics of 4H–SiC MPS with JTE at 300 K.

Figure 11 shows the simulated forward I–V of 4H–SiC MPS$_1$ ($W = 3$ μm, $S = 4$ μm, $N_{\rm A-JTE} = 1.62 \times 10^{17}$ cm^{-3}, $L = 45$ μm) with different temperatures from 300 K–500 K. It shows that the temperature coefficient of the forward I–V changes repeatedly as the forward voltage increases. In region a (as shown in Fig. 9), the PiN junctions are still inactive and only the Schottky diode is in conduction, which exhibits a positive temperature coefficient. In region b, the resistance of the N-epilayer is the dominant factor, which is characterized by a negative temperature coefficient. In region c, the PN portion is firstly activated at 575 K and the current increasing with temperature exhibits a positive temperature coefficient. We can see that the activation of the PN portions is strongly dependent on the operation temperature. This effect is important since SiC MPS devices are usually designed for applications at high temperatures.

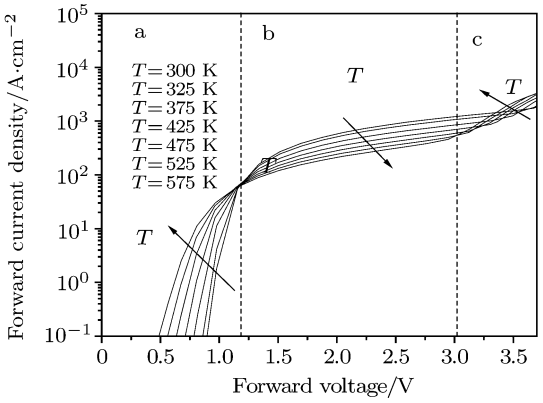


Fig. 11. Simulated forward I–V of MPS$_1$ for different temperatures.

To study the temperature sensitivity dependence of the structure size W and S on the forward I–V behaviour, the forward I–V of the MPS$_2$ ($W = 3.5$ μm, $S = 3.5$ μm, $N_{\rm A-JTE} = 1.62 \times 10^{17}$ cm^{-3}, $L = 45$ μm) and MPS$_3$ ($W = 4$ μm, $S = 3$ μm, $N_{\rm A-JTE} = 1.62 \times 10^{17}$ cm^{-3}, $L = 45$ μm) at different temperatures from 300 K–500 K is illustrated in Figs. 12(b) and 12(c), and a comparison of the forward I–V characteristics of MPS$_1$ is shown in Fig. 12(a). It is noted that the temperature sensitivity of the forward I–V of 4H–SiC MPS with JTE is strongly related to the sizes of W and S. We can see from Fig. 12(a) that the PN portion of the MPS$_1$ is always inactive until about 2.9 V from 300 K to 525 K, while the PN junctions of MPS$_2$ begin to be activated at about 2.7 V in the condition of 525 K as shown in Fig. 12(b) and those of MPS$_3$ begin to be activated at about 2.6 V in the condition of 325 K as shown in Fig. 12(c). This demonstrates that the activation of the PN junctions in 4H–SiC MPS not only depends on the structure parameters and the applied voltage but also on temperature. So at high operation temperature, the 4H–SiC MPS with larger size W and smaller size S can achieve a lower ON–resistance and give better forward I–V behaviour, while at room temperature, the 4H–SiC MPS with smaller size W and larger size S is a better choice. Therefore the operation temperature of the 4H–SiC MPS must be considered in the optimal design of devices.

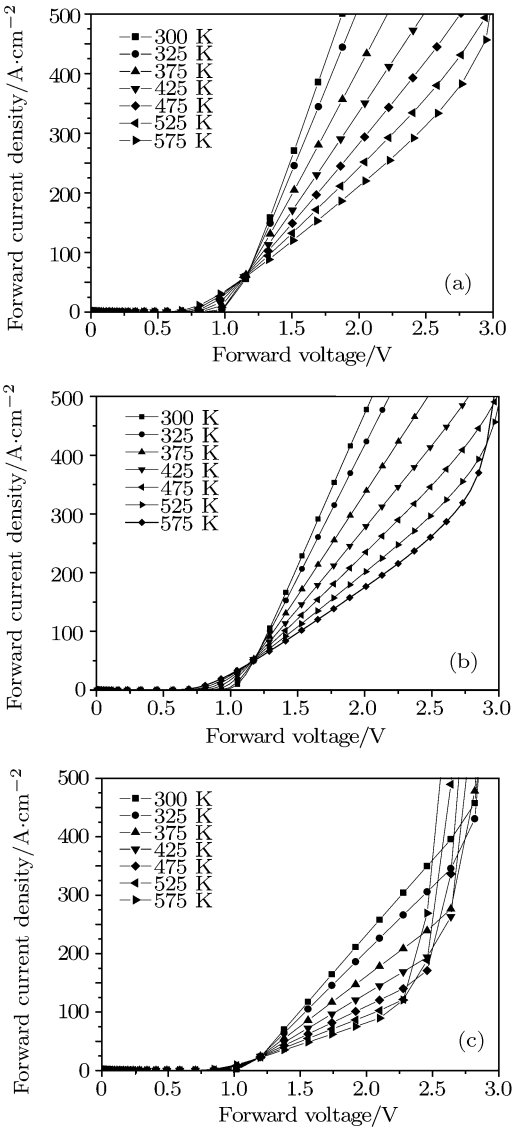


Fig. 12. Simulated forward I–V of MPS$_1$ (a), MPS$_2$ (b) and MPS$_3$ (c) from 300 K to 575 K.

4. Conclusion

In this paper we have systematically studied the design and optimization of JTE for 4H–SiC high voltage MPS by extensive numerical simulations. The in-

fluences of the JTE doping concentration, JTE length, W and S on the blocking capacity are discussed in detail. The JTE can significantly improve the breakdown voltage by controlling the JTE concentration precisely in design and process. To achieve high breakdown voltage and small area of the device, a tradeoff between the W and length of the JTE should be considered in the optimal design of the 4H–SiC MPS.

Then the temperature sensitivity of the forward behaviours is studied in terms of the different designs of MPS with JTE. It demonstrates that the 4H–SiC MPS with larger size W and smaller size S can achieve a lower ON–resistance and give better forward I–V behaviour at high operation temperatures, while at room temperature, the 4H–SiC MPS with smaller size W and larger size S is better. Therefore the operation temperature for the power 4H–SiC MPS is an important factor to be considered in the optimal design by adjusting the geometrical parameters. Considering its power dissipation and high operational temperature, we suggest that W and S should be traded off and a suitable ratio of larger W and smaller S would be preferred. The results presented here can be useful in optimizing the design of the 4H–SiC MPS with JTE at high operation temperatures.

References

[1] Callanan R J, Aqarwal A and Burk A 2008 *34th Annual Conference of IEEE* **2885–2890**

[2] Che Y, Chen L, Lü H L, Wang Y H, Zhang Y M and Zhang Y M 2008 *Acta Phys. Sin.* **57** 3921 (in Chinese)

[3] Cao Q J, Zhang Y M and Zhang Y M 2008 *Chin. Phys.* B **17** 4622

[4] Yang L A, Zhang Y M, Yu C L and Zhang Y M 2003 *Acta Phys. Sin.* **52** 302 (in Chinese)

[5] Alexandrov P , Wright W, Pan M, Weiner M, Jia L and Zhao J H 2003 *Solid-State Electron.* **47** 263

[6] Kim S C, Bahng W, Kang I H, Joo S J and Kim N K 2008 *Proc. 26th Int. Conf. Microelectronics* Niš, Serbia 11–14 May pp. 181–184

[7] Zhao J H, Alexandrow P, Fursin L, Feng Z C and Weiner M 2002 *Electron. Lett.* **38** 1389

[8] Zhu L, Chow T P, AJones K and Agarwal A 2006 *IEEE Trans. Electron Devices* **53** 363

[9] Brosselard P, Camara N and Banu V 2008 *IEEE Trans. Electron Devices* **55** 1847

[10] *DESSIS-ISE, 2D Semiconductor Device Simulator* version 10.0 2005 *Integrated Systems Engineering*, Zurich

[11] Sheridan D C, Niu G and Cressler J D 2001 *Solid-State Electron.* **45** 1659

[12] Mahajan A and Skromme B J 2005 *Solid-State Electronics* **9** 945